Identification of fission-like events in the ^{16}O + ^{181}Ta system: Mass and isotopic yield distribution

Vijay R. Sharma,[1,*] Abhishek Yadav,[1] Pushpendra P. Singh,[2,†] Manoj K. Sharma,[3] Devendra P. Singh,[1]
Unnati,[1] R. Kumar,[4] K. S. Golda,[4] B. P. Singh,[1,‡] A. K. Sinha,[5] and R. Prasad[1]

[1]*Physics Department, A. M. University, Aligarh (U.P.)-202 002, India*
[2]*INFN-Laboratori Nazionali di Legnaro, I-35020 Legnaro, Italy*
[3]*Physics Department, S.V. College, Aligarh (U.P.), India*
[4]*NP-Group: Inter University Accelerator Centre, New Delhi-110067, India*
[5]*UGC-DAE-CSR, Bidhan Nagar, Kolkata-700 098, India*

In this paper, nuclear reaction cross sections for 24 fission-like fragments ($30 \leqslant Z \leqslant 60$) have been measured for the 6.5 MeV/A ^{16}O + ^{181}Ta system. The recoil-catcher activation technique was employed followed by off-line γ spectroscopy. The isotopic yield distributions for yttrium and indium isotopes have been obtained from the experimental data. The variance of the presently measured isotopic yield distributions have been found to be in agreement with the literature values. However, the variance of the mass distribution of fission residues has found to be narrower as compared to other relatively heavier systems. A self-consistent approach to determining the isobaric charge dispersion parameters has been adopted. The measured fission cross sections at 97 and 100 MeV are satisfactorily described by a statistical model code. An attempt has been made to explain the production cross sections of intermediate mass residues in the fission of heavy residues populated via complete and/or incomplete fusion processes.

I. INTRODUCTION

In heavy-ion (HI) interactions, fission is one of the dominant reaction mechanisms at moderate excitation energies. Recent experimental data [1,2] indicate the presence of nuclear fission even at low energies where fusion is expected to be dominant. In view of the above, study of the interplay of fusion-fission processes in heavier nuclei ($Z_P Z_T \approx 800$) has been an active area of investigation during the last decade. Reactions induced by HIs are important, as both the target and projectile are heavy ions, so they carry large input angular momentum and, therefore, the composite system can be produced with relatively high spin. Also, the de-Broglie wavelength associated with the incident HI's is comparable to the nuclear dimensions; therefore, the incident ion trajectories may be treated semiclassically. The classical trajectories of the projectiles leading to different reaction processes in the collision of energetic heavy ions with the target nucleus are found to depend on the beam energy and entrance channel mass asymmetry. On the basis of driving input angular momenta imparted to the system, the reactions may be categorized broadly into complete fusion (CF) and incomplete fusion (ICF) processes. Details of CF and/or ICF processes are given elsewhere [3–5].

Depending upon the available excitation energy and other entrance channel parameters [6,7], the compound nucleus formed via CF and/or ICF may undergo fission. The fission arises due to the decay of the excited composite system formed via complete momentum transfer from projectile to the target nucleus [called complete fusion-fission (CFF)] and/or via incomplete momentum transfer from the projectile to the target nucleus [called incomplete fusion-fission (IFF)]. Nishio [8] has also reported that fission of an incompletely fused (ICF) composite nucleus is one of the dominant processes other than fission of the composite system formed by CF at intermediate energies. These studies further indicated that reaction channels such as complete fusion-fission (CFF) and incomplete fusion-fission (IFF) residues [9–14] open up at medium bombarding energies $E/A \approx 8$ MeV. It has relevance in view of the fact that one of the most important observations in earlier studies was the discovery of asymmetric mass distribution in the low-energy fission of the majority of the actinides [15]. The asymmetric mass distribution may be explained on the basis of nuclear shell effects. Asymmetry in the mass distribution decreases with the increase in excitation energy. This may be explained as a result of gradual washing out of shell effects with increasing excitation energy of the composite system. In view of the above, the study of the dynamics of heavy-ion collisions [16–18] and systematic studies of the competition of the various reaction processes which contribute to the total reaction cross sections are of considerable importance.

As such, a program to study the dynamics of processes in the ^{16}O+^{181}Ta system has been undertaken. Excitation functions for a large number of reactions in this system were analyzed to study the complete and incomplete fusion processes in the energy range $\approx$76–100 MeV [19]. Further, experimental study for the same system has been done to interpret the competition between the CF and/or ICF through recoil range distribution (RRD) measurements [20]. A part of the data analysis involving fission events is reported in this paper. The experimental data have been analyzed to obtain isotopic yield and mass distribution of residues likely to be populated by fission.

*phy.vijayraj@gmail.com
†Present address: GSI Helmholtz Centre for Heavy Ion Research GmbH, Planckstrasse 1, D-64291 Darmstadt, Germany.
‡bpsinghamu@gmail.com

The present paper is organized as follows. The experimental details are given in Sec. II. Data analysis of production cross section of fission fragments and estimation of independent cross section from the cumulative cross section are described in Sec. III. An attempt has been made to study isotopic yield distributions of the yttrium and indium isotopes and is described in Sec. III, while Sec. IV deals with the conclusions and summary of the present work.

II. EXPERIMENTAL DETAILS AND METHODOLOGY

Experiment has been performed using $^{16}O^{7+}$ beam from 15-UD Pelletron accelerator at the Inter University Accelerator Centre (IUAC), New Delhi, the rolling method were pasted on the Al-catcher foils (prepared by the rolling method) of thickness ≈ 2.0 mg/cm^2. The thickness of the Al catcher was chosen keeping in view the fact that even the most energetic residues produced due to the complete momentum transfer may be trapped in the catcher thickness. The thicknesses of each sample and the catchers were measured by the α-transmission method in which 5.487-MeV α particles obtained from a ^{241}Am source were allowed to pass through the sample. The thicknesses of the samples were determined from the observed change in the energy of the α particles using standard stopping power values [21]. The samples and the Al catchers were cut into the size of 1.2×1.2 cm^2 and were pasted on Al holders having concentric holes of 1.0 cm diameter. The Al holder was used for rapid dissipation of heat produced during the irradiation.

The irradiations were carried out in the general purpose scattering chamber (GPSC), of 1.5 m diameter having an in-vacuum transfer facility (ITF). The samples of ^{181}Ta along with appropriate catcher foil were irradiated by 97 and 100 MeV $^{16}O^{7+}$ beams with beam currents ≈ 7 pnA. The samples along with Al-catcher foils were placed normal to the beam direction, with the sample material facing the beam so that the recoiling reaction products could be trapped in the catcher foil thickness. Keeping in view the half-lives of interest, the irradiations were carried out for ≈ 8–10 h duration. The beam flux was monitored using an ORTEC current integrator by taking into account the charge collected in the Faraday cup, placed behind the target-catcher assembly. The activities induced in the target-catcher foil assembly were followed by offline γ spectrometry. A precalibrated high-purity germanium (HPGe) γ-ray spectrometer of 100 cm^3 active volume coupled to a PC through CAMAC-based FREEDOM software [22] was used for counting. The γ-ray spectrometer was calibrated using various standard γ sources of known strengths. The geometry-dependent efficiency (G_ε) of the HPGe detector for different source-detector separations was estimated using the following relation:

$$G_\varepsilon = \frac{N_0}{N_{a0}\,\theta\,e^{-\lambda t}},\qquad(1)$$

where N_0 is the observed disintegration rate of the standard source at the time of measurement, N_{a0} is the disintegration rate at the time of manufacture, λ is the decay constant, t is the lapse time between the manufacture of the source and

the start of counting, and θ is the branching ratio of the characteristic γ rays. Further, the spectrometer resolution (full width at half maximum) was ≈ 2 keV for the 1.33-MeV γ ray of the ^{60}Co source. In the present work, the standard γ sources and irradiated target-catcher foil assemblies were counted in the same geometry in order to avoid the errors due to the solid angle effect during the counting. Attention was paid to keeping the dead time of the spectrometer $\leqslant 10\%$ by suitably adjusting the source-detector separation for each irradiated sample. The γ spectra of the samples were recorded at increasing times, keeping in view that the decay curve required analysis for identification of reaction products. A typical γ-ray spectra populated in 100-MeV $^{16}O^{7+}$ induced reactions on ^{181}Ta is shown in Fig. 1. The γ peaks shown in Fig. 1 may be assigned to fission and evaporation residues. The details of the analysis of evaporation residues are given elsewhere [19]. The preliminary identification of reaction residues has been done from their observed characteristic γ rays, which were further confirmed from their decay curve analysis. This is a very specific way to identify reaction products, because each radioactive isotope has a unique decay mode. Thus, the observed intensity of the identified γ ray is a measure of the production cross section of that particular reaction channel. Detailed analysis of experimental errors is given elsewhere [23]. The overall errors in the measured cross sections, including statistical errors, are estimated to be $\leqslant 15\%$.

III. DATA ANALYSIS : ASSIGNMENT OF FISSION-LIKE EVENTS

Our earlier studies of the $^{16}O + {}^{181}$Ta system [19,20] indicated that (i) the dominant CF and/or ICF residues produced in the interactions are ^{194g,194m,193g,193m,192g,192m}Tl, ^{193g,193m,192,191g,191m}Hg, and ^{192g,191g,190g}Au [19], (ii) the excitation functions for the production of CF residues are well reproduced by theoretical calculations based on the statistical code PACE [24], (iii) most of the residues produced by α-exit channels have contributions from ICF, (iv) the presence and relative contributions of ICF components have been further confirmed by independent experiment of the recoil range distribution measurements [20]. Further, analysis of the experimental data on the $^{16}O + {}^{181}$Ta system revealed the presence of several residues which are not expected to be populated either by CF or ICF processes. Moreover, these residues were found to have charge and atomic mass values around half of the values for the residues produced by CF and/or ICF channels, indicating the possibility of their production through fission of the composite system formed via CF and/or ICF processes. It may be pointed out that these residues were identified not only by their characteristic γ rays but also from their measured half lives. As a typical example, Fig. 2 shows the observed decay curve for an yttrium isotope (^{90m}Y). The measured half-lives of all the fission-like residues were found to be in good agreement with their literature values [25]. Nuclear data such as half-lives, γ-ray energies, etc., were taken from the Table of Isotopes [25] and Nuclear Wallet Cards [26]. The intensities of the characteristic γ lines were used to determine the production cross sections

of different fission fragments using the formulations described elsewhere [23]. The identified fission fragments are listed in the Table I, along with their spectroscopic properties. The independent and cumulative decay modes are marked by I and C, respectively, in the Table I. At 100-MeV beam energy the excitation energy (E^*) of the composite system is $\approx$67 MeV and the maximum value of the input angular momentum is (ℓ_{max}) $\approx$44$\hbar$, calculated using the expression

$$\ell_{max} = R \frac{\sqrt{2\mu(E_{c.m.} - V_C)}}{\hbar}, \tag{2}$$

where R is the radius of the composite nucleus, μ is the reduced mass, $E_{c.m.}$ is the center of mass energy, and V_C is the Coulomb barrier. Gilmore *et al.* [27] also studied the system ^{16}O+^{181}Ta using the emulsion technique. From the analysis of their data, they [27] obtained the fission fragment cross sections which, in general, agree within the experimental errors to the values obtained in the present work. However, they also indicated enhanced value for angular momenta (ℓ_{max}) $\approx$61$\hbar$ instead of 44$\hbar$. The enhancement has been attributed to the quadrupole deformation effects. In the present work, $\approx$24 fission fragments, formed as a results of the fusion-fission process, have been identified. These residues may be formed by (a) the direct fission of the CF and/or ICF residues (first chance fission) and/or (b) by the fission of CF and/or ICF residues after emission of few nucleons (second, third, etc., chance fission). As such, the measured cross-section data for a given fission fragment is the cumulative sum of their population from various decay chains that may lead to the same final product.
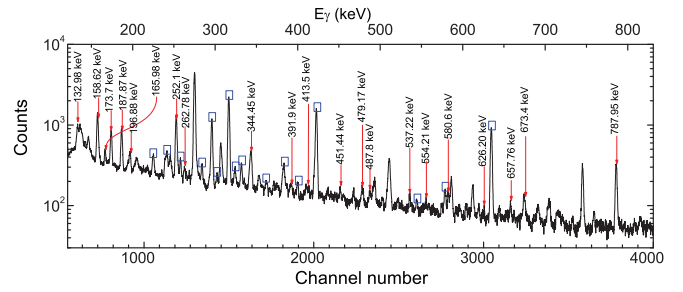
FIG. 1. (Color online) Typical γ-ray spectrum of ^{16}O + ^{181}Ta interactions at $\approx$100 MeV, where γ lines are assigned to the different reaction products expected to be populated via CFF and/or IFF processes. However, the peaks marked with blue squares correspond to the evaporation residues [19].

Measured cross sections for the identified fission fragments along with evaporation residues (ERs) [19] both at 97 and 100 MeV beam energies are given in Table II .

A. Isotopic yield distribution of In and Y

In general, for the heavy composite systems at moderate excitation energies, the nucleon emission competes directly with fission. The emission of higher charged particles is severely hindered because of the large Coulomb barrier. In such cases, nucleon emission from the fission fragments and/or the fission of successive elements of fission chains may give rise to the isotopic and isobaric distributions of the fission residues.

TABLE I. Relevant nuclear data of the fission fragments identified in the present work.

S. No.	Nuclide	E_γ (keV)	γ-ray abundance (I_γ)	Half life ($T_{1/2}$)	Fission decay mode
1	^{71}Zn^m	487.8, 120.8, 142.6	62	3.96 h	I
2	^{75}Ge	262.78	11	82.78 min	I
3	^{77}Kr	146.59	37.3	74.4 min	I
4	^{85}Y^m	787.95	1.57	4.86 h	I
5	^{86}Y	187.87	1.26	14.74 h	I
6	^{88}Kr	165.98	3.104	2.84 h	I
7	^{90}Y^m	479.17	90.2	3.19 h	C
8	^{91}Y^m	554.21	95	49.71 min	C
9	^{93}Y	266.9	7.3	10.18 h	I
10	^{105}Ru	413.5	2.27	4.44 h	I
11	^{105}In	673.4	1.70	5.07m	I
12	^{110}In	626.209	1.47	4.9 h	I
13	^{110}In^m	657.762	98	69.1 min	I
14	^{111}In^m	537.22	87	7.7 min	C
15	^{113}In^m	391.90	64.2	99.47 min	C
16	^{117}Cd	344.459	17.9	2.49 h	I
17	^{117}Sb	158.62	86	2.80 h	I
18	^{121}Xe	132.98, 252.1	2.17	40.1 min	I
19	^{129}Sb	544.7	17.9	4.40 h	I
20	^{132}La	567.17	15.7	4.8 h	I
21	^{132}Ce	451.44	2.24	3.51 h	I
22	^{132}I^m	173.7	8.8	83.7 min	C
23	^{137}Nd	580.6	13	38.5 min	I
24	^{141}Sm^m	196.88	74	22.6 min	I
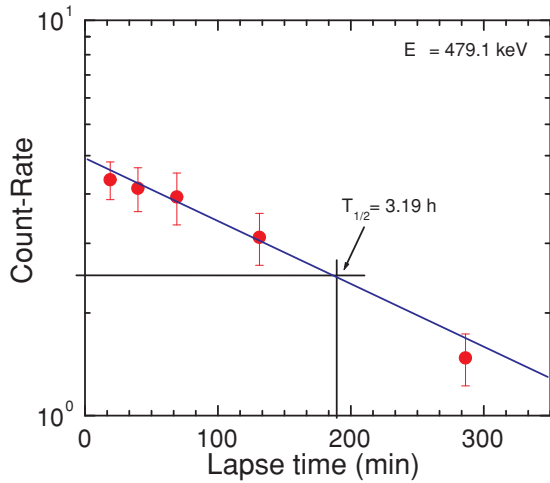
FIG. 2. (Color online) Typical decay curve of yttrium residue at $E_{\text{lab}} \approx 100$ MeV.

However, as compared to the proton emission, the emission of neutrons is more probable and therefore in most of the cases only the isotopic yield distributions are experimentally observed. The total yield of the isotopes in a decay chain of $Y^T(A)$ may be related to the corresponding primary fragments yield $Y(A')$ produced by successive neutron emission, using the relation

$$Y^T(A) = \sum_1^n P_n Y(A'), \tag{3}$$

where A' $(= A + n_{\text{avr}})$ is the mass number of the fragment emitting n number of neutrons leading to the final reaction product with mass number A. The term P_n is the probability of neutron emission from the residue with mass number A'. The Gaussian distribution for the fragment and their production yields may be related by

$$Y(A') = \frac{Y_Z}{\sqrt{2\pi\sigma_{A'}^2}} e^{-(A'-A'_p)^2/2\sigma_{A'}^2}, \tag{4}$$

here A'_p and $\sigma_{A'}^2$ are the most probable mass and the variance of the fragment isotopic yield distribution and Y_Z is the residue yield. The total yield $Y^T(A)$ of corresponding decay chain may be obtained from the yield of evaporation residues $Y(A')$ using the equation

$$Y^T(A) = \sum_{\nu=1}^n P_n \frac{Y_Z}{\sqrt{2\pi\sigma_{A'}^2}} e^{-(A'-A'_p)^2/2\sigma_{A'}^2}. \tag{5}$$

The mean-square deviation (σ_A^2) of the calculated isotopic yields $Y^T(A)$ from the experimentally determined production yields $Y^E(A)$ may be estimated by a chi-square fit, represented as

$$\chi^2 = \frac{1}{(m-p-1)} \sum_{j=1}^m \left[Y_j^T(A) - Y_j^E(A) \right]^2. \tag{6}$$

The value of chi square (χ^2) was minimized using a nonlinear least-squares fit routine, keeping the width parameter $\sigma_{A'}$ and

TABLE II. Measured cross sections of the final products formed via CF and/or ICF or via fission in the ^{16}O + ^{181}Ta reaction at $E_{\text{lab}} =$ 100 and 97 MeV.

Nuclide	$E_{\text{lab}} = 100$ MeV σ (mb)	$E_{\text{lab}} = 97$ MeV σ (mb)
^{71}Zn^m	2.6 ± 0.03	1.3 ± 0.03
^{75}Ge	23.6 ± 0.65	25.4 ± 0.90
^{77}Kr	6.5 ± 0.23	–
^{85}Y^m	27.4 ± 0.55	26.2 ± 2.45
^{86}Y	86.1 ± 12.38	60.6 ± 8.56
^{88}Kr	46.8 ± 0.44	25.4 ± 0.12
^{90}Y^m	2.3 ± 0.65	1.5 ± 0.42
^{91}Y^m	1.5 ± 0.87	0.9 ± 0.58
^{93}Y	10.4 ± 1.56	–
^{105}Ru	46.9 ± 0.35	21.5 ± 0.06
^{105}In	17.83 ± 3.566	–
^{110}In	56.2 ± 6.523	57.5 ± 0.61
^{110}In^m	1.3 ± 0.25	1.0 ± 0.03
^{111}In^m	3.5 ± 0.6	
^{113}In^m	1.22 ± 0.64	–
^{117}Cd	31.0 ± 0.59	24.2 ± 0.18
^{117}Sb	19.6 ± 1.21	10.9 ± 0.01
^{121}Xe	32.3 ± 0.50	26.6 ± 0.11
^{129}Sb	5.3 ± 0.12	4.8 ± 0.03
^{132}La	4.5 ± 2.18	–
^{132}Ce	39.8 ± 1.11	16.5 ± 0.40
^{132}I^m	1.6 ± 0.38	–
^{137}Nd	25.6 ± 0.15	7.7 ± 0.04
^{141}Sm^m	5.7 ± 0.37	3.0 ± 0.15
^{194}Tl^m (3n)	1 ± 0.1	2 ± 0.3
^{194}Tl^g (3n)	1 ± 0.1	1.5 ± 0.2
^{193}Tl^m (4n)	0.1 ± 0.01	0.1 ± 0.01
^{193}Tl^g (4n)	17 ± 2.5	15 ± 2.3
^{192}Tl^m (5n)	222 ± 33.3	171 ± 25.5
^{192}Tl^g (5n)	222 ± 33.3	171 ± 25.5
^{193}Hg^g (p3n)	10 ± 1.5	12 ± 1.7
^{193}Hg^m (p3n)	6 ± 0.5	8 ± 0.7
^{192}Hg (p4n)	154 ± 23.2	131 ± 6
^{191}Hg^g (p5n)	14 ± 2.1	7 ± 0.9
^{191}Hg^m (p5n)	18 ± 2.7	8 ± 1.2
^{192}Au^g (αn)	50 ± 7.5	63 ± 9.5
^{191}Au^g ($\alpha 2n$)	22 ± 3.2	14 ± 2.1
^{190}Au^g ($\alpha 3n$)	21 ± 3.2	40 ± 5.9

the most probable mass A'_p as free parameters using ORIGIN software. In Eq. (6) m is the number of isotopes of a given element and p is the number of free parameters, which is equal to 2 in the present case. Experimentally determined isotopic yield distributions for indium (^{105,110,110m,111m,113m}In) and yttrium (^{85m,86,90m,91m,93}Y) isotopes are plotted in the upper and lower panels of Fig 3, respectively. Since, only the metastable states of ^{111m,113m}In in indium and ^{90m,91m}Y in yttrium have been measured, the total production cross section for these isotopes will be higher than the values shown, which is indicated by upward arrows (see Fig 3). The parameters for the isotopic yield distributions were obtained by fitting the respective production cross sections to the Gaussian distribution and are given in Table III. As a typical example
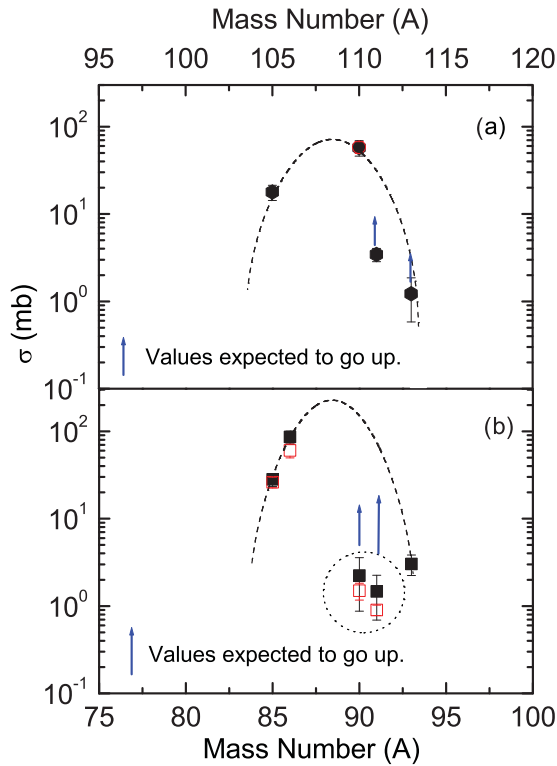
FIG. 3. (Color online) Isotopic yield distribution for (a) (^{105,110,110m,111m,113m}In) indium and (b) (^{85m,86,90m,91m,93}Y) yttrium isotopes in ^{16}O + ^{181}Ta reaction at 100 and 97 MeV, respectively.

for In isotopes, the values of $A_p \approx 108.42$ and $\sigma_A \approx 2.08$ compare well with the corresponding values of 107.88 and 2.06 reported for the ^{16}O+^{169}Tm system at $E/A \approx 5.9$ MeV by Singh *et al.* [28]. Furthermore, the variance σ_A^2 reported in the literature for a large number of other fissioning systems are also shown in Table IV , along with the presently determined values of these parameters. As can be seen from this table, the σ_A^2 values determined in the present work are close to the literature values, as expected. It may be pointed out that a Gaussian distribution for isotopic mass distribution has been observed at excitation energy ≈ 67 MeV corresponding to the incident energy ≈ 100 MeV. However, at the lower incident energy (≈ 97 MeV) only few isotopes were identified and therefore, their distribution could not be studied. For the sake of completeness, isotopes observed at ≈ 97 MeV are marked by hollow circles in Fig. 3(a) and by squares in Fig. 3(b). The isobaric charge distribution is also important in the case of fission. The isobaric charge dispersion parameter was obtained from the measured isotopic mass distribution

TABLE III. Width (σ_A) of isotopic yield distributions for different observed fission residues.

Isotope	Most probable mass A_P	Isotopic width $2\sigma_A$
Indium	108.42	4.16
Yttrium	88.41	3.45

TABLE IV. Comparison of isotopic yield distributions (σ_A^2) for different fissioning systems.

System	E^* (MeV)	Element	σ_A^2	Refs.
^{16}O + ^{181}Ta	67.041	Y	3.05 ± 0.10	a
^{16}O + ^{181}Ta	67.041	In	4.16 ± 0.01	a
^{16}O + ^{159}Tb	57.1	Sr	3.31	[28]
^{16}O + ^{159}Tb	57.1	Y	4.41	[28]
^{16}O + ^{159}Tm	61.06	In	4.24	[28]
^{16}O + ^{159}Tm	61.06	Tc	4.62	[28]
^{7}Li + ^{232}Th	41.7	Sb	4.08	[29]
^{7}Li + ^{232}Th	41.7	I	3.96	[29]
^{11}B + ^{232}Th	55.7	Sb	4.0	[30]
^{11}B + ^{232}Th	55.7	I	5.43	[30]
^{11}B + ^{232}Th	55.7	Cs	3.72	[30]
^{11}B + ^{238}U	67.4	Rb	3.84 ± 0.16	[31]
^{11}B + ^{238}U	67.4	Cs	3.95 ± 0.14	[31]
^{22}Ne + ^{238}U	64.5	Rb	4.23 ± 0.40	[31]
^{22}Ne + ^{238}U	64.5	Cs	4.26 ± 0.90	[31]
^{20}Ne + ^{208}Pb	46.4	Sb	3.43 ± 1.02	[32]
^{20}Ne + ^{208}Pb	46.4	I	3.95 ± 0.87	[32]

^{a}Present work.

using the following prescription [30]. The fractional isotopic independent yields $FY^I(Z)$ were obtained by dividing the independent yields by their corresponding charge yields. For deducing the total yield of mass A it is required to have knowledge of the isobaric charge dispersion parameter σ_Z and the most probable charge Z_p. The Z_P for the yttrium and indium isotopes are calculated using

$$Z_P(A) = \frac{Z}{A_p} A, \tag{7}$$

where Z and A are the atomic number and the atomic mass number of the fission fragment, respectively. The distribution of fractional chain yield vs the charge corrected isotopic fragments (Z-Z_P) so determined is shown in Fig. 4. The solid
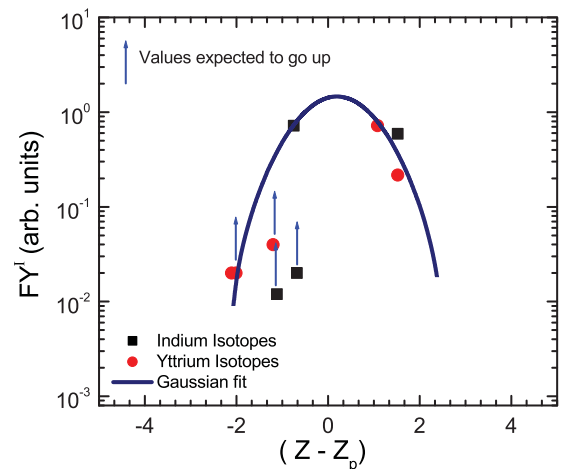
FIG. 4. (Color online) Fractional isotopic yield corresponding to corrected charge distribution.

curve of Fig. 4 is the Gaussian, given by

$$Y = \frac{1}{\sqrt{2\pi\sigma_Z^2}} e^{-(Z-Z_p)^2/2\sigma_Z^2}. \qquad (8)$$

From the above fitting procedure, the estimated isobaric charge dispersion parameter σ_Z has been found to be ≈ 0.81 charge units. The values of σ_Z have also been calculated by converting the width parameter of isotopic yield σ_A into σ_Z using

$$\sigma_Z = \frac{\sigma_A \cdot Z}{A_p} \qquad (9)$$

The calculated average value of width parameter σ_Z is found to be ≈ 0.85 charge units, which is in good agreement with the value obtained from the corrected charge distribution plot (Fig. 4). The above method indicates self-consistency of the present analysis.

B. Mass distribution of fission fragments in ^{16}O + ^{181}Ta reaction

Mass distribution is one of the important observables directly related to the collective dynamics of fission processes [33,34]. Activities measured in the catcher foils were used for the mass distribution studies. The plots of experimentally determined production cross sections (given in Table IV of various fission fragments at two different energies ($E_{\text{lab}} = 97$ and 100 MeV) are shown in Figs. 5(a) and 5(b). The upward arrows indicate that only the metastable states have been measured and
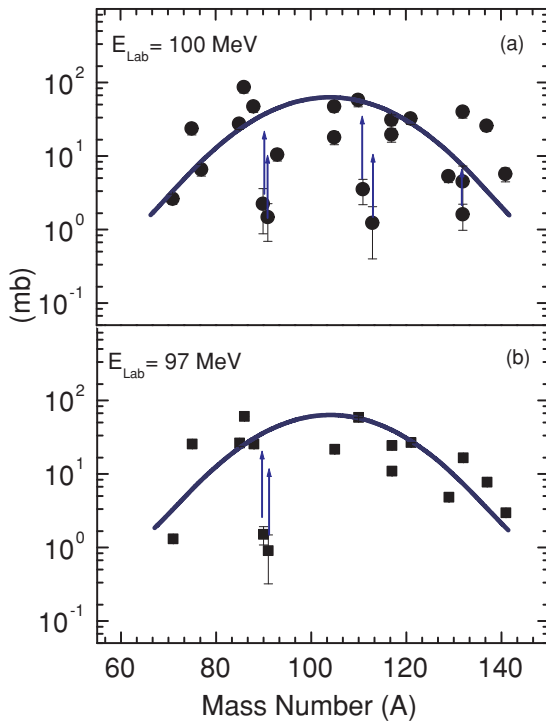
the total production cross sections of these fission fragments are expected to increase. These distributions were found to be symmetric, in general, as expected. Stability (stiffness) of the fissioning nucleus to mass-asymmetric deformation can be understood through observed mass distribution. To understand this aspect, Itkis *et al.* [35] and Rusanov *et al.* [36] analyzed a large collection of data over a wide range of fissility of the compound nucleus at medium excitation energies. The calculated centroid, width, and variance of the mass distribution obtained in the present experiment were compared with the values reported in the literature for similar systems [37–41]. The mass distribution width σ_M (≈ 12.6 mass units) reported by Hinde *et al.* [37] for fission of ^{201}Tl is found to agree with the present measurements involving the nearby isotope ^{197}Tl. Variance of fission fragment mass distribution for the same projectile (^{16}O) and different targets as a function of mass asymmetry ($\mu = M_T/M_{T+P}$) of interacting systems, taken from the literature, are shown as a bar diagram in Fig. 6. It may be observed from Fig. 6 that variance increases with mass asymmetry of the interacting ions.

The experimental total fission cross section σ_f^T was obtained by adding the measured cross sections for individual fission fragments. The value of σ_f^T at 97 and 100 MeV beam energies are found to be ≈ 315 and ≈ 500 mb. The total fission cross section has also been theoretically estimated using the statistical code ALICE [42], which employs a rotating liquid drop model [43]. In the present calculations, the fission barrier B_L^f is taken as ≈ 18 MeV and $a_f/a_n = 1.2$ (where a_f and a_n are the level-density parameters for fission and neutron emissions, respectively). The calculated σ_f^T (theory) are found to be ≈ 500 and ≈ 680 mb at energies 97 and 100 MeV, respectively. There is reasonable agreement in the theoretically calculated and experimentally measured fission cross section. However, presently measured total fission cross sections are relatively higher than the value obtained from angular distribution measurements [44]. Gilmore *et al.* [27] also measured the total fission cross section for the same system and obtained values, e.g., ≈ 300 and ≈ 430 mb at 97 V and

FIG. 5. (Color online) Mass distribution of fission products in ^{16}O + ^{181}Ta reaction at (a) $E_{\text{lab}} = 100$ MeV and (b) $E_{\text{lab}} = 97$ MeV, respectively. Upward arrows indicate values expected to go up. The lines are drawn through the data points for Gaussian fit.
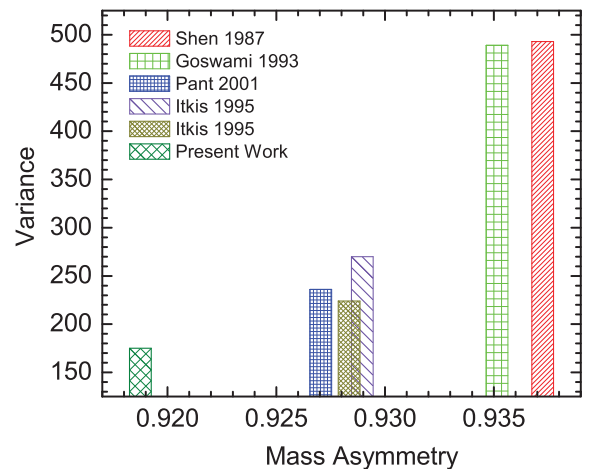
FIG. 6. (Color online) Mass asymmetry vs variances for the same projectile and different target combinations (Shen 1987 [39], Goswami 1993 [40], Pant 2001 [38], and Itkis 1995 [41]).
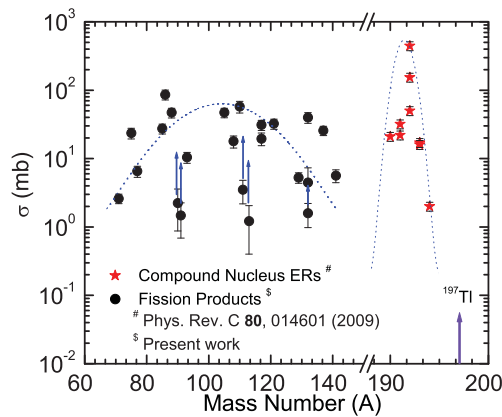
FIG. 7. (Color online) Schematic picture of fission fragments and compound nucleus evaporation residues at $E_{\mathrm{lab}} \approx 6.5/n$. The dotted lines are drawn through the data points to guide the eyes.

100 MeV, respectively, which are in reasonable agreement with the present measurements. Figure 7 shows the distribution of cross sections for all the residues identified in the present experiment. In principle, the cross section vs mass distributions for heavy-ion interactions may have three components due to (i) CF and/or ICF residues, (ii) fission-like residues, and (iii) few nucleon transfer residues or projectile-like fragments (PLFs). In Fig. 7, the peak at higher mass number may be attributed to the residues formed by CF and/or ICF processes, while the broad peak in the intermediate mass region may be assigned to fission events. The PLFs could not be detected

in the present experiment because of their relatively higher energy and generally very short life times.

IV. SUMMARY AND CONCLUSIONS

In the present work, several fission residues in the system $^{16}\mathrm{O} + ^{181}\mathrm{Ta}$ at 97 and 100 MeV were identified and their production cross sections obtained. The data were analyzed to deduce parameters for isotopic yield and isobaric charge distributions. Mass distribution of the fission fragments was also obtained. The isotopic yield distributions are satisfactorily reproduced by Gaussian distribution. The distribution parameters obtained from the present measurements agree reasonably well with the literature values. The analysis of the data further indicates that the mass asymmetry of the interacting ion has considerable influence of fission probabilities. The total fission cross section obtained from the present measurements agrees with some earlier measurements as well as with those calculated using angular momentum dependent rotating liquid drop fission barrier.

[1] L. Shvedov, M. Colonna, and M. Di Toro, Phys. Rev. C **81**, 054605 (2010).

[2] H. Q. Zhang, C. L. Zhang, C. J. Lin, Z. H. Liu, F. Yang, A. K. Nasirov, G. Mandaglio, M. Manganaro, and G. Giardina, Phys. Rev. C **81**, 034611 (2010).

[3] P. P. Singh *et al.*, Phys. Lett. B **671**, 20 (2009).

[4] P. P. Singh *et al.*, Phys. Rev. C **80**, 064603 (2009).

[5] P. P. Singh *et al.*, J. Phys.: Conf. Ser. **282**, 012019 (2011).

[6] W. J. Swiatecki, Phys. Scr. **24**, 113 (1981).

[7] C. Gregoire, C. Ngo, and B. Remaud, Phys. Lett. B **99**, 17 (1981).

[8] K. Nishio, H. Ikezoe, Y. Nagame, M. Asai, K. Tsukada, S. Mitsuoka, K. Tsuruta, K. Satou, C. J. Lin, and T. Ohsawa, Phys. Rev. Lett. **93**, 162701 (2004).

[9] J. V. Kratz, J. O. Liljenzin, A. E. Norris, and G. T. Seaborg, Phys. Rev. C **13**, 2347 (1976).

[10] D. J. Hinde, J. R. Leigh, J. J. M. Bokhorst, and J. O. Newton, Nucl. Phys. A **472**, 318 (1987).

[11] J. P. Lestone, J. R. Leigh, J. O. Newton, and J. X. Wei, Nucl. Phys. A **509**, 178 (1990).

[12] M. C. Duh, H. Baba, N. Takashi, A. Yokoyama, and T. Saito, Nucl. Phys. A **550**, 281 (1992).

[13] A. Pagano, S. Aiello, E. De Filippo, G. Lanzano, S. Lo Nigro, C. Milone, G. Blancato, G. Di Marco, and M. C. Mermaz, Phys. Rev. C **47**, 1170 (1993).

[14] G. K. Gubbi, A. Goswami, B. S. Tomar, B. John, A. Ramaswami, A. V. R. Reddy, P. P. Burte, and S. B. Manohar, Phys. Rev. C **53**, 796 (1996).

[15] R. Tripathi and A. Goswami, Eur. Phys. J. A **26**, 271 (2005).

[16] R. L. Kozub, N. H. Lu, J. M. Miller, D. Logen, T. W. Debiak, and L. Kowalski, Phys. Rev. C **11**, 1497 (1975).

[17] J. B. Natowitz, E. T. Chulick, and M. N. Namboodiri, Phys. Rev. C **6**, 2133 (1972).

[18] R. Broda, M. Ishihara, B. Herskind, H. Oeschler, S. Ogaza, and R. Ryde, Nucl. Phys. A **248**, 356 (1975).

[19] D. P. Singh *et al.*, Phys. Rev. C **80**, 014601 (2009).

[20] D. P. Singh *et al.*, Phys. Rev. C **81**, 054607 (2010).

[21] SRIM06; [http://www.srim.org/].

[22] FREEDOM: Data Acquisition and Analysis System designed to support the accelerator-based experiments at the Inter University Accelerator Centre, New Delhi, India.

[23] V. R. Sharma, M.Phil. dissertation, A.M. University, Aligarh, Inida, 2011.

[24] A. Gavron, Phys. Rev. C **21**, 230 (1980).

[25] E. Brown and R. B. Firestone, *Table of Isotopes* (Wiley, New York, 1986).

[26] J. K. Tuli, Nuclear Wallet Card, National Nuclear Data Center, Brookhaven National Laboratory, Upton, NY, 2000.

[27] J. Gilmore, S. G. Thompson, and I. Perlman, Phys. Rev. **128**, 2276 (1962).

[28] P. P. Singh, B. P. Singh, B. Sharma, Unnati, M. K. Sharma, R. Prasad, R. Kumar, and H. D. Bhardwaj, Int. J. Mod. Phys. E **17**, 549 (2008).

[29] R. Tripathi, K. Sudarshan, S. Sodaye, B. S. Tomar, G. K. Gubbi, A. Goswami, A. V. R. Reddy, and S. B. Manohar, Radiochem. Acta **90**, 185 (2002).

[30] G. K. Gubbi, A. Goswami, B. S. Tomar, A. Ramaswami, A. V. R. Reddy, P. P. Burte, S. B. Manohar, and B. John, Phys. Rev. C **59**, 3224 (1999).

[31] M. de *et al.*, Phys. Rev. C **14**, 2185 (1976).

[32] R. Tripathi, K. Sudarshan, A. Goswami, P. K. Pujari, B. S. Tomar, and S. B. Manohar, Phys. Rev. C **69**, 024613 (2004).

[33] A. C. Berriman, D. J. Hinde, M. Dasgupta, C. R. Morton, R. D. Butt, and J. O. Newton, Nature (London) **413**, 144 (2001).

[34] D. J. Hinde, A. C. Berriman, R. D. Butt, M. Dasgupta, I. I. Gontcher, C. R. Morton, A. Mukherjee, and J. O. Newton, J. Nucl. Radiochem. Sci. **3**, 31 (2002).

[35] M. G. Itkis, Yu. A. Muzychka, Yu. Ts. Oganessian, V. N. Okolovich, V. V. Pashkevich, A. Ya. Rusanov, V. S. Salamatin, G. N. Smirenkin, and G. G. Chubarian, Phys. At. Nucl. **58**, 2026 (1995).

[36] A. Ya. Rusanov, M. G. Itkis, and V. N. Okolovich, Phys. At. Nucl. **60**, 683 (1997).

[37] D. J. Hinde, D. Hilscher, H. Rossner, B. Gebauer, M. Lehmann, and M. Wilpert, Phys. Rev. C **45**, 1229 (1992).

[38] L. M. Pant, R. K. Choudhury, A. Saxena, and D. C. Biswas, Eur. Phys. J. A **11**, 47 (2001).

[39] W. Q. Shen *et al.*, Phys. Rev. C **36**, 115 (1987).

[40] A. Goswami, A. V. R. Reddy, B. S. Tomar, P. P. Burte, and S. B. Manohar, Radiochem. Acta **62**, 173 (1993).

[41] M. G. Itkis *et al.*, in *European Physical Society XV Nuclear Physics Divisional Conference on Low Energy Nuclear Dynamics*, edited by Yu. Ts. Oganessian (World Scientific, Singapore, 1995), p. 177.

[42] F. Plasil and M. Blann, Phys. Rev. C **11**, 508 (1975).

[43] S. Cohen, F. Plasil, and W. J. Swiatecki, Ann. Phys. (NY) **82**, 557 (1974).

[44] B. R. Behera, S. Roy, P. Basu, M. K. Sharan, S. Jena, M. Satpathy, S. K. Datta, L. Satpathy, and M. L. Chatterjee, Pramana J. Phys. **53**, 3 (1999).